Changing human upper-limb synergies with an exoskeleton using viscous fields

Vincent Crocher, Nathanaël Jarrassé, Anis Sahbani, Agnès Roby-Brami and Guillaume Morel

Abstract— **Robotic exoskeletons can apply forces distributed on the limbs of the subject they are connected to. This offers a great potential in the field of neurorehabilitation, to address the impairment of interjoint coordination in hemiparetic stroke patients. In these patients, the normal flexible joint rotation synergies are replaced by pathological fixed patterns of rotation. In this paper, we investigate how the concept of synergy can be exploited in the control of an upper limb exoskeleton. The long term goal is to develop a device capable of changing the joint synchronization of a patient performing exercises during rehabilitation.**

The paper presents a controller able of generating joint viscous torques in such a way that constraints on joint velocities can be imposed to the subject without constraining the hand motion. On another hand, the same formalism is used to describe synergies observed on the arm joint motion of subjects realizing pointing tasks.

This approach is experimented on a 4 Degrees Of Freedom (DoF) upper arm exoskeleton with subjects performing pointing 3-dimensional tasks. Results exhibit the basic properties of the controller and show its capacity to impose an arbitrary chosen synergy without affecting the hand motion.

I. Introduction

For several years, robotic devices have been developed for rehabilitation applications, particularly for neurorehabilitation for post-stroke patient. The main contribution of rehabilitation robots is to assist active movements of the patients by providing the ability of finely controlling forces and movements in a repetitive manner. Robotics show promising clinical results [1]. Considering specifically upper-limb rehabilitation, some devices, like the MIT Manus, are already used in clinics [2]. However, little is known about the mechanism of their effects and many questions remain open. Is the clinical benefit only quantitative by affording a longer and more intense therapy [2] ? What are the most pertinent robotic architectures and modes of control [3] ? What are the clinical indications as a function of the individual patients needs [4], [5] ? A fundamental aspect, here, is for the robot to be able of responding to any patients movement, thanks to fine control of the mechanical interaction with the limb [6]. While the pioneer devices were aimed at controlling only the hand motion in a plane, many exoskeletons have now been developed with the capacity of 3D interaction at joint level. Representative examples include SUEFUL 7 [7], the 4-DoF Delaware exoskeleton [8], Rupert [9], ARMin [10], [11] or CEA-LIST ABLE [12], which is the 4-DoF exoskeleton used for the experiments in this paper. Most of the controllers proposed in the literature consist of adapting solutions developed for endpoint interaction to the joint space of the exoskeleton [13], [11]. However, few control laws entirely exploit the ability of an exoskeleton to control simultaneously several joints in correspondence with human motor control.

V. Crocher, N. Jarrassé, A. Sahbani and G. Morel are with Institute of Intelligent Systems and Robotics (CNRS - UMR 7222), University Pierre & Marie Curie, Paris, France crocher,jarrasse,sahbani,morel@isir.upmc.fr

A. Roby-Brami is with Laboratory Neurophysics and Physiology (CNRS - UMR 8119), University Paris Descartes, France agnes.roby-brami@univ-paris5.fr

II. Human motor coordination

Human motor system is largely redundant, in particular the structure of the upper-limb. In the neuroscience literature, the term synergy is used to designate solutions found by the CNS to solve kinematic redundancy during motions [16]. Synergies have three essential properties: the sharing pattern of rotations; flexibility allowing automatic compensation between elements and task dependency [14]. The sharing pattern of rotation can be mathematically described thanks to the principal component analysis (PCA). Given the space E of redundant kinematic variables coding a given human motion, only a small subspace of E is explored during natural movements. This subspace, which dimension corresponds to the number of DoF required for the task, is spanned by a few orthogonal vectors (the Principal Components (PCs)) that can be computed from recording the human motion during experiments. PCA was applied to several groups of movements corresponding to a given task. PCA used in the joint position space showed that a large part of variance in multiple joint rotations can be explained by a limited number of components [review in [14]]. For example, considering upper-limb movements, respectively 3 and 2 principal components (PCs) may explain more than 85% of the variance in 10 DoF for catching objects [15] or pointing in 3D [16].

Redundancy is also of primary importance in upper arm rehabilitation. Inter-joint coordination is severely perturbed in hemiparetic patients after a stroke related cerebral lesion. They show abnormal synergies which clinically appear as stereotyped and global patterns of movement triggered by any effort to move [17]. In addition, quantified kinematic analysis showed that their shoulder-elbow coordination was disrupted with difficulties to both couple and decouple appropriately joint rotations as a function of task requirements [18], [19]. Clinical recovery is probably linked to

the reacquisition of a better pattern of synergies [20] in particular after robotic therapy [21].

The formalism of PCA has also been exploited for the command of robotic hands [22], [23].

Due to its linear nature, the PCA can be equivalently used in the joint position space or in the joint velocity space. Lacquaniti and Soechting described by the synchronization of rotation velocity between two DoF [24]. Although, to the authors knowledge, the literature did not fully explore PCA in joint velocity space [25]. In the context of robot control, using velocities instead of positions is interesting, because it allows for expressing viscous fields rather than elastic fields, which would require to exploit a reference trajectory, namely a prediction of the subjects motion [26]. The present paper explores the idea that active interaction at joint level during unperturbed hand movements could be an interesting rationale for rehabilitation of stroke patients in order to cope with the question of redundancy. Practically such a command would allow either to train the correct pattern or conversely to produce excessive errors according to the hypothesis that the patient will benefit from the adaptation [27].

III. Proposed viscous control law

In [26] a control law is proposed aimed at applying a viscous field in order to impose to the subject a given way of synchronizing joint movements. This section summarizes how this controller works.

We consider an exoskeleton with n_r active joints, connected to the upper limb of a subject. The subject is asked to perform a task, *e.g.* a pointing task, which imposes m DoFs. We consider a redundant configuration, characterized by $m < n_r$. Therefore, there is an infinite number of solutions in the joint space that satisfy the task constraints.

We note $\dot{\mathbb{Q}}$ the robot joint velocity space of dimension n_r. The controller proposed in [26] is aimed at keeping the robot joint velocities in a subspace of $\dot{\mathbb{Q}}$ defined by a set of $l = n_r - m$ constraints. The constraint is expressed by:

$$\mathbf{C}\dot{\mathbf{q}} = 0 \tag{1}$$

with $\mathbf{C} \in \mathbb{R}^{l \times n_r}$.

At each moment, if the robot joint velocity $\dot{\mathbf{q}}$ belongs to the chosen subspace, it is orthogonal to $\mathbf{C}$ and then $\mathbf{C}\dot{\mathbf{q}} = 0$. In this case, the exoskeleton shall apply no resistive torque. Otherwise, a torque has to be generated to correct current velocity. This torque is proportional to the projection of $\dot{\mathbf{q}}$ on the constraint $\mathbf{C}$:

$$\tau_{c1} = -b\mathbf{C}^{+}\mathbf{C}\dot{\mathbf{q}} \quad , \tag{2}$$

where b is a scalar viscosity factor and $\mathbf{C}^{+}$ is the pseudo-inverse of the matrix $\mathbf{C}$:

$$\mathbf{C}^{+} = \mathbf{C}^{\mathrm{T}}\left(\mathbf{C}\mathbf{C}^{\mathrm{T}}\right)^{-1} \quad . \tag{3}$$

We notice that in general, the exoskeleton dissipates energy, *i.e.* $\tau_{c1}^{\mathrm{T}}\dot{\mathbf{q}} < 0$. In order to compensate this dissipation, we introduce a second term noted τ_{c2}. This second torque is calculated from a projection on the orthogonal direction to the constraint:

$$\tau_{c2} = b\alpha\left(\mathbf{I} - \mathbf{C}^{+}\mathbf{C}\right)\dot{\mathbf{q}} \quad , \tag{4}$$

where α is a scalar modulation. Large values of α would lead to instability because a large positive feedback would be induced. In our case, α is computed in order to obtain no energy dissipation:

$$\left(\tau_{c1} + \tau_{c2}\right)^{\mathrm{T}}\ \dot{\mathbf{q}} = 0 \quad . \tag{5}$$

Solving equation (5), we obtain :

$$\alpha = \begin{cases} 0 \text{ if } \left(\dot{\mathbf{q}}^{\mathrm{T}}\mathbf{C}^{+}\mathbf{C}\dot{\mathbf{q}} - \|\dot{\mathbf{q}}\|^2 = 0\right) \\ \\ \frac{\dot{\mathbf{q}}^{\mathrm{T}}\mathbf{C}^{+}\mathbf{C}\dot{\mathbf{q}}}{\dot{\mathbf{q}}^{\mathrm{T}}\mathbf{C}^{+}\mathbf{C}\dot{\mathbf{q}} - \|\dot{\mathbf{q}}\|^2} \text{ otherwise} \end{cases} ; \tag{6}$$

For the experiments presented in this paper, a coefficient $\varepsilon \in [0, 1]$ is added to allow the modulation of τ_{c2} in the controller and evaluate its effect. The final controller is thus:

$$\tau_c = -b\left[\mathbf{C}^{+}\mathbf{C} + \varepsilon\alpha\left(\mathbf{I} - \mathbf{C}^{+}\mathbf{C}\right)\right]\dot{\mathbf{q}} \quad . \tag{7}$$

The behavior of this controller is in Fig. 1 for a simple case where $n_r = 2$, $l = 1$ and $m = 1$, $\mathbf{C} = [-1\ 3]$ and $\varepsilon = 1$.

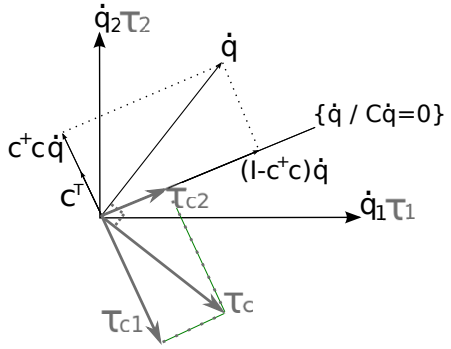

Fig. 1. Representation of the projections in the case of $C = [-1\ 3]$.

In [26], the controller is validated for a 4-DoF exoskeleton ($n_r = 4$) and 3-DoF pointing tasks ($m = 3$). An arbitrary value is used for $\mathbf{C}$, imposing a particular synchronization between two joints. In this paper, the question of defining constraints from the observation of human synergies is studied.

IV. Defining constraints $\mathbf{C}$ from the observation of human movements

Exploiting the controller (7) requires to define the constraint $\mathbf{C}$. In this section, it is shown that Eq. (1), which has been used to define $\mathbf{C}$ from the control point of view, is also a mathematical way to describe human upper limb natural synergies.

A. Computing a robot joint posture compatible with a measured human posture

A first problem to be solved when trying to define constraints in the robot joint space from the observation of human movements is the computation of a robot joint configuration that is compatible with a given observed human posture. More precisely, given a human arm posture, defined by the joint position vector $\mathbf{q}_h \in \mathbb{R}^{n_h}$, the question to be solved here is how to compute a robot posture $\mathbf{q}_r \in \mathbb{R}^{n_r}$ that is kinematically compatible. In the general case, the kinematics of the robot and those of the human limb differ. Therefore, $\mathbf{q}_r \neq \mathbf{q}_h$. In fact, even their dimension differ for most of the existing exoskeletons ($n_r \neq n_h$). This is why a specific procedure was developed to compute $\mathbf{q}_r$ from the subject's motion recordings.

A first step is to ensure that a solution $\mathbf{q}_r$ exists for any possible posture of the subject's arm, providing that it fits in the exoskeleton workspace. This pertains to the exoskeleton design, and to the way the exoskeleton is mechanically coupled to the subject's limb. In a previous paper [28], a general method was proposed to design passive mechanisms to be placed between the active robot and splints worn by the subject in order to guarantee *isostaticity*. An example of these passive mechanisms is presented on Fig. 2 for ABLE exoskeleton. Thanks to these mechanisms, the forces applied to the limb through the splints are proven to be fully controllable. Dually, it is equivalent to state that for any motion of the splints worn by the subject, it exists a compatible motion of the exoskeleton. It can be computed in the following way.

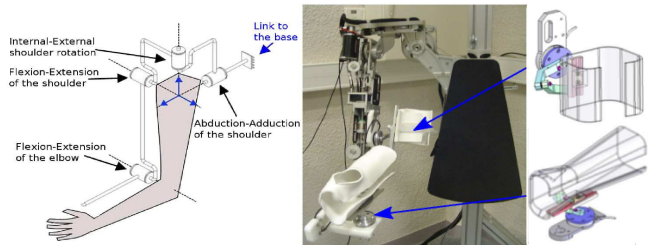

Fig. 2. ABLE with the two splints, the two passive mechanisms and the two F/T sensors (at exoskeleton/passive mechanisms interaction points).

With the proposed design method, one can define for the robot an augmented joint vector $\mathbf{q}_t^{\mathrm{T}} = [\mathbf{q}_r^{\mathrm{T}}\ \mathbf{q}_l^{\mathrm{T}}]^{\mathrm{T}}$, where $\mathbf{q}_l$ is the n_l dimensional joint position of the passive mechanisms used to connect the robot to the splints installed on the subject (see Fig. 2). The method [28] imposes that:

$$dim(\mathbf{q}_r) + dim(\mathbf{q}_l) = n_r + n_l = 6n\ , \tag{8}$$

where n is the number of connexions. Furthermore, the method also guarantees a full kinematic rank. In other words, if the translational and rotational velocities of the n splints with respect to the base body are grouped into a $6n$-dimensional vector $\dot{\mathbf{x}}$, then the mapping

$$\dot{\mathbf{x}} = J(\mathbf{q}_t)\dot{\mathbf{q}}_t \tag{9}$$

is non singular.

Therefore, computing $\mathbf{q}_r$ compatible with any human arm posture pertains to standard inverse kinematics of a $6n$ joint robot. Namely, the following procedure is used:

1) Motion recording: the subject is wearing the splints that will be mechanically connected to the robot; from an external motion tracking system, the position and orientation of the splints with respect to the robot base body are recorded. This provides $\mathbf{x}(t)$.
2) An inverse kinematic model is used to compute $\mathbf{q}_t(t)$ corresponding to $\mathbf{x}(t)$. A standard approach can be used.
3) $\mathbf{q}_r$ is simply extracted from $\mathbf{q}_t$ with $\mathbf{q}_r = [\mathbf{I}_{n_r}\ \mathbf{0}_{n_l}]\,\mathbf{q}_t$

B. Applying PCA to the robot joint velocities

Now that we are able of computing, for any human arm movement, a corresponding robot joint configuration, it is interesting to study these variables, and the way they are coordinated when a subject executes a task in a redundant situation.

To that purpose, we focus in the next on 3D pointing tasks without constraints on the hand orientation. Namely, subjects are asked to touch several 3D targets placed in front of them with a stick attached to their forearm. Since there is no constraint on the stick orientation, the task dimension is 3. During the motion, the splint positions and orientations are recorded and converted into $\mathbf{q}_r(t)$. Then, time differentiation and filtering are operated to finally obtain $\dot{\mathbf{q}}_r(t)$. Finally, PCA is performed on the recorded joint velocities.

From this analysis, 4 principal components are identified, in such a way that:

$$\dot{\mathbf{q}}_r(t) = \sum_{i=0}^{4} c_i(t)\mathbf{p}_i \tag{10}$$

where $\mathbf{p}_i$ are the principal components and $c_i(t)$ their respective weight during the motion.

Classically, synergies are characterized, within the PCA framework by the fact that less than 4 principal components are sufficient to *explain* most of the movement. Namely:

$$\dot{\mathbf{q}}_r(t) \approx \sum_{i=0}^{d} c_i(t)\mathbf{p}_i \tag{11}$$

where $d < 4$. In the next, we describe the experiments that were conducted in order to evaluate if PCA was an appropriate tool for characterizing synergies in the joint velocity space during 3D pointing tasks. Through these experiments, we want to verify that only 3 PCs are sufficient to describe movements without loosing information. This question is investigated under two conditions: when the subject is connected to the robot controlled to apply a null torque, or when he/she is not connected to the robot. The robot used for the experiments is the 4-DoF ABLE exoskeleton [12] presented on Fig. 2.

The study is realized with 4 male right-handed healthy subjects (age : 23-28). For each subject the protocol is divided into two parts.

In a first time, the subject is seated on a stool, with two splints, one on the arm, one on the forearm fitted with CODAmotion® markers, without robot (see Fig. 3). The markers positions recorded during movements are then used to reconstruct the corresponding robot joints values along the trajectory using the method described in part IV-A. The subject is asked to successively perform 3 different tasks :

1) In the first task, the subject is asked to move freely and make arbitrary movements in the whole workspace in front of him.
2) In the second one, the subject is asked to point successively at 8 different targets in front of him, arranged in 2 rows, from a unique starting point placed beside the subject thigh.
3) In the third task, the subject is asked to point many times at the same target in front of him, from the same starting point than in task 2.

Each task lasts 30 seconds.

In a second time, the subject is installed in the exoskeleton, attached thanks to the 2 splints (see Fig. 3) and is asked to repeat the 3 tasks. The exoskeleton control consists here in an active gravity compensation of its own weight.

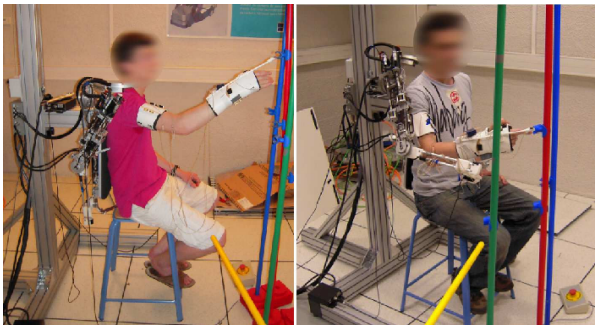

Fig. 3. Subjects pointing targets, without and with the exoskeleton.

For each task and each subject, a PCA is done on exoskeleton joints velocity data. From these analysis 4 PCs are extracted. Then the percentage of representativity of each PC is calculated. This representativity, averaged for the 4 subjects, is presented on Fig. 4 for each different case (with and without robot, for each different task).

For the first task, consisting in arbitrary movements, we validate that 3 PCs represent typically 90% of the joint velocity variance. Note that random values would lead to 25% for each PC, but obviously the subjects execute arbitrary movements that are not random.

In the case of pointing towards one or several targets, the first 3 components explain more than 98% of the variance, whatever the condition. At a maximum, only 2% of variance could be lost if we consider only 3 PCs to describe the joint velocities. It is interesting to notice that for all the tasks the

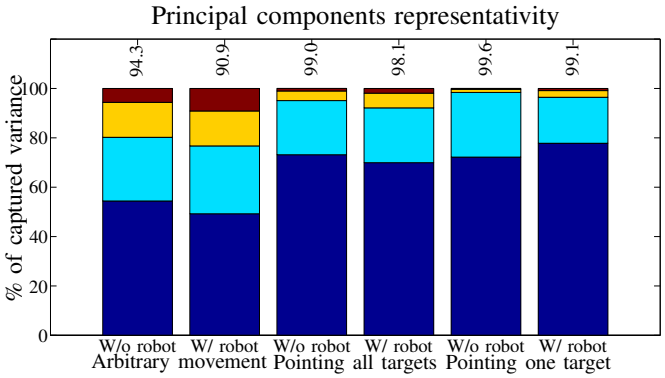

Fig. 4. Percentage of representativity of each PCs, and percentage for the first 3, for each case, averaged for the 4 subjects.

percentage of the movement that is not explained by the three mains PCs is always sensibly smaller with the robot than without the robot. This could be explained by the friction of the different exoskeleton axis.

Most importantly, PCA confirms to be an adequate tool for the description of synergies in the joint velocity space for pointing tasks. In other words, if $\mathbf{p}_4$ is the fourth PC, one has:

$$\dot{\mathbf{q}}_r(t) = \sum_{i=0}^{4} c_i(t)\mathbf{p}_i \approx \sum_{i=0}^{3} c_i(t)\mathbf{p}_i \quad \Rightarrow \mathbf{p}_4^{\mathrm{T}}\dot{\mathbf{q}}_r \approx 0 \qquad (12)$$

In other words, $\mathbf{p}_4^{\mathrm{T}}$ can be viewed as a constraint that characterizes pointing movements for a given human being. It is expressed in the same way as Eq. (1) which describes the constraints that the robot can apply. In the next, we will define the *natural constraint* $\mathbf{C}_n$ by:

$$\mathbf{C}_n := \mathbf{p}_4^{\mathrm{T}} \ . \qquad (13)$$

When the exoskeleton is programmed with $\mathbf{C} = \mathbf{C}_n$, it is supposed to impose a constraint that corresponds to the one naturally employed by the subject. Therefore, the exoskeleton should not modify the subject's motion. On the contrary, when $\mathbf{C} \neq \mathbf{C}_n$, a modification of the joint synchronization should be observed.

V. Experiments on Joint Synergies Modification

In order to evaluate the capacity of the 4-DoF active exoskeleton to modify the upper-limb joint coordinations, a number of experiments were done. The study was carried out by three young right-handed healthy subjects (age: 21-24): two males and one female. For each subject the natural constraint vector, noted $\mathbf{C}_n$, was determined as explained in the previous section. To achieve the exoskeleton evaluation a protocol was defined for the experiments. It evaluates the effect of τ_{c1} and τ_{c2} defined in Eq. (7).

1) Step 1: *Natural constraint mode*
   Only the dissipative torque (τ_{c1} presented in equation 3) is applied in this mode. It allows to check whether the natural constraint $\mathbf{C}_n$ was satisfied. The viscous coefficient k is set to 1.0 Nm.s/rad.

2) Step 2: *Non-natural hard constraint mode*
In this mode, the natural constraint $\mathbf{C}_n$ for each subject was slightly modified. The modified constraint is noted $\mathbf{C}_m$. Only the dissipative torque τ_{c1} is applied. k is also set to 1.0 Nm.s/rad.
3) Step 3: *Non-natural soft constraint mode*
We apply in this mode the same constraint used in the previous step. The stiffness coefficient used in τ_{c1} is modified in order to evaluate its impact. k is set to 0.4 Nm.s/rad. This mode could be seen as a soft constraining one.
4) Step 4: *Non-natural constraint mode with non-dissipative torque*
This mode aims to satisfy the modified constraint $\mathbf{C}_m$ (presented in step 2) by applying the global torque defined in equation 7. Compared to the previous steps, the non-dissipative torque τ_{c2} is introduced. k is set to 0.4 Nm.s/rad and ε is set to 0.8.

For the four steps of the protocol, the subject is installed in ABLE exoskeleton and is asked to point four targets in front of him, with a rod attached to his arm. Targets are materialized by a point on a rod. The first three targets are placed at 30° one from each other at elbow height, and the fourth one is placed in front of the subject 20cm higher. Each pointing starts at a fixed reference point beside the subject thigh and he is asked to reach each target five times.

Robot data (joint positions/speeds/torques, and torques/forces from sensors) are recorded at 100 Hz. For each mode i ($i \in \{1, ..., 4\}$) of the protocol, PCA is done on joint speeds and the less weighted PC is kept and labeled as "observed constraint". This constraint is noted $\mathbf{C}^i_{obs}$. Table I presents a summary of the different modes.

Mode	Applied constraint	k	ε	Observed constraint
1	$\mathbf{C}_n$	1.0	0	$\mathbf{C}^1_{obs}$
2	$\mathbf{C}_m$	1.0	0	$\mathbf{C}^2_{obs}$
3	$\mathbf{C}_m$	0.4	0	$\mathbf{C}^3_{obs}$
4	$\mathbf{C}_m$	0.4	0.8	$\mathbf{C}^4_{obs}$

TABLE I
SUMMARY OF THE DIFFERENT CONTROL MODES

Finally, a CODAmotion® system records the position of the end-point of the human arm for each step of the protocol.

A. Evaluation Metric

In order to evaluate if the applied non-natural constraint $\mathbf{C}_m$ is well respected by the subject, we introduce a measure function $\psi(\mathbf{a}, \mathbf{b})$, defined for two unit vectors $\mathbf{a}$ and $\mathbf{b}$ as follows:

$$\psi(\mathbf{a}, \mathbf{b}) = 1 - \mathbf{a}^{\mathrm{T}}\mathbf{b} \quad . \tag{14}$$

This function is zero if the vectors are collinear ; increasing values of ψ indicates an increasing difference between the 2 vectors until $\psi = 1$ when they are orthogonal.

Based on ψ function and for each mode i, we introduce a deviation ratio, noted r_i. It is given by:

$$\forall i \in \{2, 3, 4\}, \qquad r_i = \frac{\psi\left(\mathbf{C_m}, \mathbf{C^i_{obs}}\right)}{\psi\left(\mathbf{C_n}, \mathbf{C_m}\right)} \tag{15}$$

$\psi\left(\mathbf{C_n}, \mathbf{C_m}\right)$ represents the amount of deviation between the natural and the modified constraints, noted "*imposed deviation*". $\psi\left(\mathbf{C_m}, \mathbf{C^i_{obs}}\right)$ represents the subject deviation regarding the modified constraint. So, the ratio r_i indicates whether the subject respects the applied constraint while taking into account the importance of the imposed deviation.

B. Experimental results

We evaluate in this section if the applied synergy constraint is well respected while keeping the same hand trajectory. Energy dissipation and applied forces using the proposed control law are also discussed.

Subject	$\psi(\mathbf{C}_n, \mathbf{C}_m)$	r_2	r_3	r_4
1	6.6×10^{-2}	7.5%	7.8%	3.6%
2	1.5×10^{-1}	2.2%	1.8%	3.8%
3	9.6×10^{-2}	1.0%	6.2%	5.3%
Mean	1.0×10^{-1}	3.6%	5.2%	4.2%

TABLE II
ψ AND RATIO VALUES IN DIFFERENT MODES

The second column of table II presents the imposed deviation for each subject. The natural constraint is deviated in average by 10%. For the three non-natural constraints, the computed ratio does not overpass an overage of 6% which means that the measured deviation does not exceed 6% of the imposed one. These results prove that the imposed constraints are well respected by the subjects.

For each mode, joint velocities are also analyzed using PCA. Fig. 5 illustrates the obtained results. This diagram confirms the satisfaction of the constraints. For all modes of the protocol, the three selected PCs represent at least 99.8% of the movement variance.

Registered hand trajectory for subject 1, using CODAmotion®, are illustrated in Fig. 6. Data are presented for the four targets averaged over the five trials. Despite constraint modification (natural synergy and so natural joint speed modification), a small deviation is observed. For the three subjects, the mean deviation is 3.5cm for global movements of about 50cm.

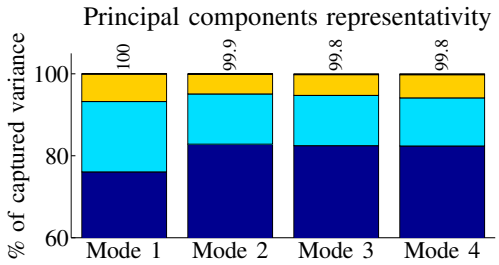

Fig. 5. Percentage of representativity of each PCs, and percentage for the first 3, for each mode, averaged for the 3 subjects.

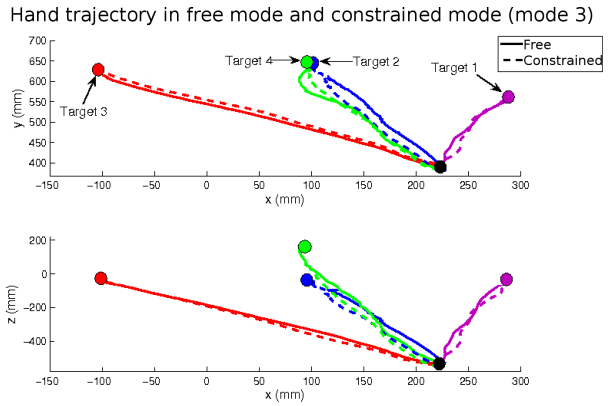

Fig. 6. Hand trajectory recorded with CODAmotion® system for subject 1 for free movements and for constrained movements (mode 3) for the 4 targets. Projections in X-Y and X-Z plans.

As illustrated in Fig. 2, two force/torque sensors are placed at the two interaction points between the exoskeleton and subject upper-limb (arm and forearm). For subject 1, measured forces are averaged over the five trials for each mode. Fig. 7 presents the mean of forces levels during each mode. In mode 1, the force levels are about 3N whereas they are about 5N in the 3 other modes. It proves that the natural constraint, imposed by the control law, is naturally respected by the subject. Motion correction by the exoskeleton stills low in this mode. Whereas, in mode 2, 3 and 4, when a non-natural constraint is imposed, the measured force levels are clearly higher. In these modes, exoskeleton/subject interaction are more important in order to satisfy the imposed new coordination.

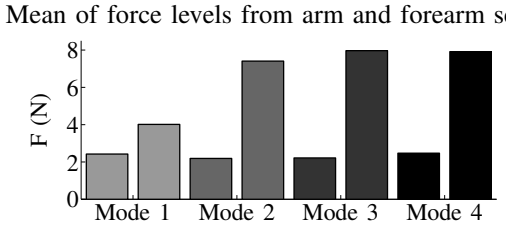

Fig. 7. Mean of force levels for each force/torque sensor (arm and forearm) measured in each mode for the subject 1.

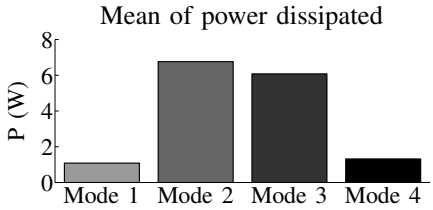

Fig. 8. Mean of the power dissipated in each mode, averaged for the all targets and the 3 subjects.

Finally, the second torque of the control law τ_{c2} (described in equation 4) is designed to encourage the correct motion and to reduce the energy dissipation. The later could be given by $P = \tau_{\mathbf{c}}{}^{\mathrm{T}}\dot{\mathbf{q}}$. For each mode, Fig. 8 presents the average of the energy dissipated over the three subjects. This energy decreases significantly in mode 4 regarding mode 3. Mode 4 corresponds to the step of the protocol where τ_{c2} is added while keeping the same stiffness of τ_{c1} than the mode 3. So, the second torque clearly reduces the energy dissipation. In addition, it does not interfere with the subject movement. A quick look at the last column of table II confirms the respect of the imposed constraint.

VI. CONCLUSIONS AND FUTURE WORKS

In this paper, we extended principal component analysis on joint position to joint velocity space in order to express upper-limb synergies. This extension was experimented on healthy subjects and was proved for a large workspace in the case of pointing tasks. Using this analysis, the dimension of the movement subspace was reduced to the task dimension. The useless dimensions are used to express motion constraints.

In addition, the control law presented in this paper is able to impose non-natural synergies (expressed as motion constraints) to healthy subjects without disturbing their hand motion. Experiments conducted using a 4-DoF exoskeleton, showed the efficiency of our approach.

Several studies will be conducted with more subjects in order to investigate in more depth the ability of the control law to modify a synergy, with different parameters. Experiments with post-stroke patients are being planned, in a first step without the robot, to perform PCA on joint velocities any verify that a reduction of the joint space dimension applies. The application of non natural constraint to these patients will be the next step. An interesting property of the proposed controller is that this can be done very progressively. Indeed, changes in the constraint are fully programmable and can be as little as wanted.

VII. ACKNOWLEDGMENTS

The support of the French National Agency for research, ANR, program PSIROB-ROBO-0003, to the Brahma Project is gratefully acknowledged.

REFERENCES

[1] G. Kwakkel, B.J. Kollen, and H.I. Krebs. Effects of Robot-Assisted therapy on upper limb recovery after stroke: A systematic review. *Neurorehabil Neural Repair*, 22(2):111–121, April 2008.

[2] Bruce T. Volpe, Daniel Lynch, Avrielle Rykman-Berland, Mark Ferraro, Michael Galgano, Neville Hogan, and Hermano I. Krebs. Intensive sensorimotor arm training mediated by therapist or robot improves hemiparesis in patients with chronic stroke. *Neurorehabilitation and Neural Repair*, 22(3):305 –310, May.

[3] L. Marchal-Crespo and D.J. Reinkensmeyer. Review of control strategies for robotic movement training after neurologic injury. *Journal of neuroengineering and rehabilitation*, 6(1):20, 2009.

[4] A.A.A. Timmermans, H.A.M. Seelen, R.D. Willmann, and H. Kingma. Technology-assisted training of arm-hand skills in stroke: concepts on reacquisition of motor control and therapist guidelines for rehabilitation technology design. *Journal of NeuroEngineering and Rehabilitation*, 6(1):1, 2009.

[5] R. Riener, M. Frey, M. Bernhardt, T. Nef, and G. Colombo. Human-centered rehabilitation robotics. In *Proceedings of the 9th International Conference on Rehabilitation and Robotics*, pages 319–22, 2005.

[6] N. Maclean, P. Pound, C. Wolfe, and A. Rudd. Qualitative analysis of stroke patients' motivation for rehabilitation. *British Medical Journal*, 321(7268):1051, 2000.

[7] R.A.R.C. Gopura, K. Kiguchi, and Yang Li. SUEFUL-7 : a 7DOF upper-limb exoskeleton robot with muscle-model-oriented EMG-based control. In *Intelligent Robots and Systems, 2009. IROS 2009. IEEE/RSJ International Conference on*, pages 1126–1131, 2009.

[8] EA Brackbill, Y. Mao, SK Agrawal, M. Annapragada, and V.N. Dubey. Dynamics and Control of a 4-dof Wearable Cable-driven Upper Arm Exoskeleton. 2009.

[9] J. He, EJ Koeneman, RS Schultz, DE Herring, J. Wanberg, H. Huang, T. Sugar, R. Herman, and JB Koeneman. RUPERT: a device for robotic upper extremity repetitive therapy. In *Engineering in Medicine and Biology Society, 2005. IEEE-EMBS 2005. 27th Annual International Conference of the*, pages 6844–6847, 2005.

[10] T. Nef and R. Riener. ARMin–design of a novel arm rehabilitation robot. In *Rehabilitation Robotics, 2005. ICORR 2005. 9th International Conference on*, pages 57–60, 2005.

[11] M. Mihelj, T. Nef, and R. Riener. A novel paradigm for patient-cooperative control of upper-limb rehabilitation robots. *Advanced Robotics*, 21(8):843–867, 2007.

[12] P. Garrec, JP Friconneau, Y. Measson, and Y. Perrot. ABLE, an innovative transparent exoskeleton for the upper-limb. In *IEEE/RSJ International Conference on Intelligent Robots and Systems, 2008. IROS 2008*, pages 1483–1488, 2008.

[13] C.R. Carignan, M.P. Naylor, and S.N. Roderick. Controlling shoulder impedance in a rehabilitation arm exoskeleton. In *IEEE International Conference on Robotics and Automation Pasadena*, 2008.

[14] M.L. Latash. *Synergy*. Oxford University Press, USA, 2008.

[15] Till Bockemhl, Nikolaus F. Troje, and Volker Drr. Inter-joint coupling and joint angle synergies of human catching movements. *Human Movement Science*, 29(1):73–93, February 2010.

[16] G. Hoffmann, I. Laffont, S. Hanneton, and A. Roby-Brami. How to extend the elbow with a weak or paralyzed triceps: control of arm kinematics for aiming in C6-C7 quadriplegic patients. *Neuroscience*, 139(2):749–765, 2006.

[17] S. Brunnström. *Movement therapy in hemiplegia: a neurophysiological approach*. Facts and Comparisons, 1970.

[18] M.F. Levin. Interjoint coordination during pointing movements is disrupted in spastic hemiparesis. *Brain*, 119(1):281, 1996.

[19] D.S. Reisman and J.P. Scholz. Aspects of joint coordination are preserved during pointing in persons with post-stroke hemiparesis. *Brain*, 126(11):2510, 2003.

[20] A. Roby-Brami, A. Feydy, M. Combeaud, EV Biryukova, B. Bussel, and MF Levin. Motor compensation and recovery for reaching in stroke patients. *Acta neurologica scandinavica*, 107(5):369–381, 2003.

[21] L. Dipietro, HI Krebs, SE Fasoli, BT Volpe, J. Stein, C. Bever, and N. Hogan. Changing motor synergies in chronic stroke. *Journal of Neurophysiology*, 98(2):757, 2007.

[22] C. Brown and H. Asada. Inter-finger coordination and postural synergies in robot hands via mechanical implementation of principal components analysis. In *IEEE-RAS Intl. Conf. on Intelligent Robots and Systems*, page 28772882, 2007.

[23] Giulia Matrone, Christian Cipriani, Emanuele Secco, Giovanni Magenes, and Maria Carrozza. Principal components analysis based control of a multi-dof underactuated prosthetic hand. *Journal of NeuroEngineering and Rehabilitation*, 7(1):16, 2010.

[24] F. Lacquaniti and JF Soechting. Coordination of arm and wrist motion during a reaching task. *Journal of Neuroscience*, 2(4):399, 1982.

[25] S. Micera, J. Carpaneto, F. Posteraro, L. Cenciotti, M. Popovic, and P. Dario. Characterization of upper arm synergies during reaching tasks in able-bodied and hemiparetic subjects. *Clinical Biomechanics*, 20(9):939–946, 2005.

[26] V. Crocher, A. Sahbani, and G. Morel. Imposing joint kinematic constraints with an upper limb exoskeleton without constraining the hand motion. In *To appear in the IEEE/RSJ International Conference on Intelligent Robots and Systems (IROS'10)*, Taipei, Taiwan, 2010.

[27] J.L. Patton, M.E. Stoykov, M. Kovic, and F.A. Mussa-Ivaldi. Evaluation of robotic training forces that either enhance or reduce error in chronic hemiparetic stroke survivors. *Experimental Brain Research*, 168(3):368–383, 2006.

[28] N. Jarrasse and G. Morel. On the kinematic design of exoskeletons and their fixations with a human member. In *Proceedings of Robotics: Science and Systems*, Zaragoza, Spain, June 2010.